



Final Draft of the original manuscript

Gnedenkov, A.; Lamaka, S.; Sinebryukhov, S.; Mashtalyar, D.;
Egorin, V.; Imshinetskiy, I.; Zavidnaya, A.; Zheludkevich, M.;
Gnedenkov, S.:

**Electrochemical behaviour of the MA8 Mg alloy in minimum
essential medium.**

In: Corrosion Science. Vol. 168 (2020) 108552.

First published online by Elsevier: 19.02.2020

<https://dx.doi.org/10.1016/j.corsci.2020.108552>

Electrochemical behaviour of the MA8 Mg alloy in minimum essential medium

A.S. Gnedenkov^{a,□}, S.V. Lamaka^b, S.L. Sinebryukhov^a, D.V. Mashtalyar^{a,c}, V.S. Egorkin^{a,c},
I.M. Imshinetskiy^a, A.G. Zavidnaya^a, M.L. Zheludkevich^{b,d}, S.V. Gnedenkov^{a,c}

^a *Institute of Chemistry of FEB RAS, 159 Pr. 100-letiya Vladivostoka, Vladivostok, 690022, Russia*

^b *Magnesium Innovation Centre – MagIC, Institute of Materials Research, Helmholtz-Zentrum Geesthacht (HZG), 21502 Geesthacht, Germany*

^c *Far Eastern Federal University, 8 Sukhanova St., Vladivostok, 690950, Russia*

^d *Institute for Materials Science, Faculty of Engineering, Kiel University, Kiel, Germany*

Abstract

The difference of the protective properties of the corrosion film formed on the MA8 Mg alloy in the mammalian cell culture medium (MEM) and 0.83 wt. % NaCl solution is established using OCP, PDP and EIS tests. The impedance modulus in the frequency range from 10^5 Hz down to 10^{-1} Hz for the sample immersed in MEM is higher than that for the sample immersed in NaCl solution. Ca and P rich deposits are formed in the corrosion layer on the Mg alloy in MEM. The model of the corrosion mechanism for MA8 Mg alloy in the MEM is proposed.

Keywords: A. Magnesium; A. Alloy; B. EIS; B. Raman spectroscopy; C. Oxide coatings

1. Introduction

Magnesium and its alloys are considered as materials for bioresorbable implants, which eliminate the need for a second surgical procedure for implant removal [1]. Such materials have important advantages when compared to both degradable polymers and other metals, e.g. similar mechanical properties to the bone [2]. Even more, magnesium has a stimulating effect on the growth of a new tissue due to its functional role and natural presence in bone [3].

Advances in magnesium alloy corrosion and biocorrosion were summarized by Esmaily et al. [4] who indicated that due to the high complexity of the interactions between Mg and the biological surroundings, many open questions still exist, especially regarding detailed mechanistic understanding.

To promote the biomedical application of Mg-based materials, it is important to study the kinetics and mechanism of the corrosion in the environment, which imitates the human body media. Such approach will facilitate understanding of the surface processes and behaviour of bioresorbable materials.

Therefore, multiple studies investigate the influence of different media components on the corrosion activity and mechanism of the magnesium degradation. In [5] it has been shown that co-precipitation of Ca and P containing dense layer of hydroxyapatite-like corrosion products stabilizes the local pH values in the range of 8.0 to 8.5 and slows down the degradation rate of Mg alloys exposed to Ca^{2+} containing HBSS electrolyte. In the follow up work [6], it has been shown by means of EIS that formation of this dense hydroxyapatite layer occurs exclusively in presence of HPO_4^{2-} , HCO_3^- and Ca^{2+} . If at least one of these components is missing in the electrolyte, the protective properties of formed corrosion products

[□] - Corresponding author. Tel: +8 4232215284; fax: +8 4232312590;
E-mail: asg17@mail.com (A.S. Gnedenkov).

are much weaker. Synthetic pH buffers, HEPES [5] and TRIS [6] were found to greatly (up to 10 times) accelerate degradation rate of Mg alloys.

Many researcher groups used the electrochemical impedance spectroscopy (EIS) and potentiodynamic polarization (PDP) to study the corrosion activity during magnesium biocorrosion. Chen et al. [7] used EIS and SEM to elucidate the formation mechanism of the surface coatings on the binary Mg-14Li alloy and their role in regulating degradation of the underlying Mg-14Li sample in a carbonate-rich simulated body fluid, i.e. MEM, in comparison with two generic biocompatible Mg alloys (Mg-0.5Zn-0.5Ca and Mg-3Al-1Zn). It was proposed that the single-phase structure and formation of protective and defect-free Li_2CO_3 film give rise to the controlled and homogenous corrosion behaviour of Mg-14Li in MEM, providing new insights for the exploration of biodegradable Mg materials [7]. However, this study only shows the influence of carbonate ions on the corrosion propagation of the Mg alloy and does not give a complete picture of the influence of various MEM species on the evolution of protective properties of the formed surface film.

Rondelli et al. [8] used EIS technique to study the electrochemical behaviour of Ni-free austenitic stainless steel for orthopaedic applications using four different test solutions: phosphate-buffered saline (PBS), MEM, MEM + 10 % fetal calf serum (FCM), MEM + 10 % fetal calf serum + L929 fibroblast cell line (Cell). The resistance of the inner film, directly related to the material's uniform corrosion resistance, raised with the immersion time and increased in the following order: $\text{PBS} < \text{FCS} \approx \text{Cell} < \text{MEM}$. At the same time, this work concentrated on electrochemical calculation and does not show detailed information about chemical changes of the surface layer of studied material.

The effect of different amount of Ca in Mg-Zn-RE- x Ca ($x = 0, 0.5, 1.5, 3$ and 6) alloy on its *in vitro* corrosion behaviour in a Kokubo simulated body fluid was investigated by Bakhsheshi-Rad et al. [9] using EIS and PDP. According to results obtained, the corrosion current density of Mg-Zn-RE alloy decreased after addition of 0.5 wt. % Ca whilst further addition of Ca from 1.5 to 6 wt.% significantly increased the corrosion current density of the ternary Mg-Zn-RE alloy. However, the authors do not specify the difference in the corrosion mechanism of Ca-containing Mg alloys in other physiological solutions.

In the research [10], the effect of the presence of living cells (SaOS-2) on *in vitro* degradation of Mg-2.0Zn-0.98Mn (ZM21) magnesium alloy was examined by two methods simple immersion/cell culture tests and electrochemical measurements (EIS and PDP) under cell culture conditions. Electrochemical measurements revealed the presence of living cells increased corrosion current density and decreased polarization resistance after 48 h of incubation. Acceleration of ZM21 corrosion can be attributed to the decrease of medium pH due to cellular metabolic activities. At the same time, this work does not provide the detailed analysis of the corrosion products formed on the magnesium alloy.

Liu et al. [11] studied the *in vitro* degradation behaviour of Mg-Ca alloy in the presence of albumin using in-situ observation, hydrogen evolution method and EIS technique. The corrosion and hydrogen evolution rates decreased and the formation of filiform corrosion induced by Cl^- was inhibited due to the adsorption of albumin molecule. Moreover, the higher the concentration of albumin, the higher is the inhibitive effect. The EIS results showed that addition of albumin enhanced the charge transfer resistance

and film resistance at the open-circuit potential. However, this study does not show the synergetic influence of other compounds presented in simulated body solutions on the corrosion degradation of Mg-based samples.

Kim et al. [12] used EIS and PDP to reveal the increase of the corrosion resistance of the polycaprolactone and zinc oxide nanoparticles (ZnO NPs) electrospun composite coatings on the AZ31 Mg alloys in SBF solution as compared to the resistance of bare and only polymeric coated samples. EIS data indicated that with the increase in the content of ZnO NPs in the composite coatings increased the corrosion resistance. This work focused on studies of the coating adhesion, its composition, electrochemical properties and biocompatibility, though, the surface characterization after corrosion tests was missed.

In the work [13] the authors used EIS to characterize the degradation performance of the biodegradable Mg–Y–Zn alloys in SBF solution buffered with HEPES. The EIS measurements revealed increasing polarization resistance with increasing Y content, which was attributed to the beneficial influence of Y on the corrosion resistance of Mg alloys [14]. In the research [15], the EIS result showed the formation of biodegradable calcium phosphate coating could protect the Mg–Nd–Zn–Zr alloy substrate and improve its corrosion resistance in Hank's solution. The detailed analysis of the corrosion products formed on the Mg alloy surface after *in vitro* and *in vivo* studies in conjunction with corrosion mechanism description would significantly improve these works.

PDP and EIS were applied to study the corrosion behaviour of Ca-P contained micro-arc oxidation (MAO) coating, pulse electrodeposited Ca-P coating, strontium phosphate conversion coating and the Mg-Sr alloy in Hank's solution [16]. The MAO coating showed the slowest degradation performance among these three coatings, which was reflected by better corrosion behaviour examined by electrochemical test. This study dealt with protective properties investigation of the formed coatings in correlation with cell assays while missing the chemical analysis of the sample after immersion test, which could promote the understanding the process of the material biodegradation.

EIS and PDP tests were used to characterize the corrosion performance of MAO coatings on AZ31 Mg alloy in simulated body fluid vs. Earle's Balance Salt Solution (EBSS) [17]. It was found that thicker MAO coating (produced by a higher voltage process) had higher electrochemical impedance. The PDP and EIS scans showed a similar trend, indicating that the samples in EBSS were less corroded than in SBF. However, the results of this work do not provide a comprehensive explanation of the role and influence of individual ions of simulated body solutions on the corrosion process of Mg sample.

In [18–22] the authors have established that use of physiological solutions, which have similar composition to blood plasma is essential for *in vitro* studies of the Mg corrosion in the human body. In our previous study [23], we pointed out the specificity of magnesium degradation in cell culture medium – MEM (minimum essential medium) as compared to Mg corrosion in trivial NaCl. We have detected the higher hydrogen evolution rate for the sample immersed in 0.83 % NaCl solution in comparison with MEM. It was established that protective magnesium-substituted hydroxyapatite layer formed on the sample during immersion in MEM stabilizes the local pH of MEM near 8.0 (according to scanning ion-selective electrode technique) and slows down the Mg degradation. At the same time, using scanning

vibrating electrode technique we found higher electrochemical activity for the samples in MEM than in NaCl solution at the initial stage of the material immersion. This can be related to the effect of lactic acid formed as a result of bacteria metabolism in non-sterile conditions or gluconic acid in MEM. It was indicated that corrosion process as well as corrosion of the MA8 magnesium [24–29] sample in MEM occurs in a rather complex way and obeys more complicated mechanism in comparison with typical Mg alloy corrosion in NaCl solution. That study mainly focused on the localized electrochemical studies (measurements of pH and current density distribution) of the Mg-based material degradation.

Up to date, there are still unsolved points concerning the specificity of corrosion of Mg and its alloys *in vitro* conditions. The comprehension of features of the corrosion mechanism of biodegradable magnesium-based materials will sufficiently stimulate their utilization in the implantation sphere.

Hence, the present work describes the evolution of protective properties of the surface film formed on MA8 Mg alloy during immersion in MEM in comparison with 0.83 % NaCl solution. The distinct tendencies of corrosion process development in two different media were established. The surface analysis of the corrosion product film formed on the material surface in MEM as well as the model of the Mg alloy corrosion mechanism were provided. This work is the continuation of our previous study [23] connected with detailed analysis of the electrochemical behaviour of the biodegradable magnesium sample in the solution with the composition similar human blood plasma. The results of the present study promote understanding of the corrosion mechanisms of magnesium alloys used as biodegradable implants.

In this work, in order to make differentiation between corrosion degradation and electrochemical activity of the samples in MEM as well as to study the formation of the corrosion layer we used global electrochemical techniques like EIS and PDP in conjunction with Raman spectroscopy and SEM-EDX analysis of specimens with corrosion products precipitation.

2. Experimental

2.1. Samples

The plates of magnesium alloy MA8 (1.5–2.5 wt. % Mn; 0.15–0.35 wt. % Ce; 0.05 wt. % Fe; 0.1 wt. % Si; 0.007 wt. % Ni; 0.1 wt. % Al; 0.05 wt. % Cu; 0.002 wt. % Be; 0.3 wt. % Zn; balance – Mg) were used for this study. The presence of iron as impurities increases the corrosion rate of magnesium alloys [30,31]. The addition of Mn as an alloying element by the developers of the alloy is aimed at reducing the effect of Fe on the corrosion rate [4,32,33]. Manganese forms with iron intermetallic compounds and phases (α -Fe(Mn), β -Mn(Fe)), which impede the depolarization of the microscopic cathodes (impurities) [34]. All plates were mechanically ground using SiC papers, polished with Aluminum Oxide Lapping Films (Thorlabs Inc., USA) with the grain size down to 3 μ m. Ethanol was used for lubrication during the polishing. After the polishing, the plates were washed with deionized water, degreased with ethanol and dried in air.

MA8 magnesium alloy specimens were studied in MEM (# 61100 powder, Gibco[®], Thermo Fisher Scientific, USA) [35,36] with addition of 2.2 g L⁻¹ NaHCO₃ [37] (pH 7.40) and in 0.83 % NaCl solution (Na⁺ and Cl⁻ concentrations are similar to the human blood plasma [18]).

2.2 Electrochemical measurements

Electrochemical activity of the MA8 Mg alloy plates was studied using PDP and EIS methods by means of the electrochemical system 12558WB («Solartron Analytical», UK), consisted of electrochemical interface SI 1287 and frequency response analyzer FRA 1255B connected with the PC. Electrochemical tests were carried out in MEM and NaCl solutions in a three-electrode cell Model K0235 Flat Cell («PAR», USA) at room temperature. The Mg alloy plates of a size of 15 mm × 20 mm × 1.5 mm for electrochemical measurements were used. In all our experiments the exposed area of the specimens to electrolyte solution was equal to 1 cm². Saturated calomel electrode (SCE) Hg/Hg₂Cl₂, KCl (potential versus normal hydrogen electrode was equal to 0.248 V) was used as a reference electrode. The platinum mesh was used as a counter electrode. Before the electrochemical tests (EIS, PDP), the plates were immersed in MEM and NaCl solution for 60 min to stabilize the electrode potential. The open circuit potential (OCP) was recorded. The PDP measurements were carried out at a sweep rate of 1 mV s⁻¹. DC potentiodynamic polarization measurements were performed according to the ASTM G5-14 standard [38–40]. The Mg alloy specimens were polarized in the anodic direction from the potential of $E = E_C - 350$ mV up to $E = E_C + 900$ mV. The Levenberg-Marquardt (LEV) method was used to calculate the values of corrosion potential, E_C , corrosion current density, I_C , in potential range from $E_C + 100$ mV down to $E_C - 250$ mV in accordance with the equation (1):

$$I = I_C (10^{(E-E_C)/\beta_a} + 10^{-(E-E_C)/\beta_c}). \quad (1)$$

According to the previous studies [41,42] the LEV method enables one to obtain the best fit values of E_C and I_C as well as the slopes of the cathodic, β_c , and anodic branch, β_a .

It should be noted that Tafel equation cannot be directly applied for Mg-based systems. Tafel only works for the systems controlled by the charge transfer. In the case of the metallic surfaces covered with the protective layers of products, the Tafel equation cannot be used. Especially it is truth for the anodic part, which is fully dominated by the IR drop through the film until its breakdown. Therefore we also used the recommended modified procedure [43,44] on the base of the theory of McCafferty [45] and Leroy [46] when only intersection of the extrapolated cathodic linear region with E_C is taken in order to estimate the I_C .

The sinusoidal signal with the 10 mV (rms) amplitude was used for EIS measurements. The spectra were acquired at an OCP in the frequency range from 0.1 MHz down to 0.1 Hz at logarithmic sweep 10 points per decade. CorrWare/Zplot software was used to control the experiment. PDP and EIS data were processed using CorrView/ZView software. To study the electrochemical behaviour evolution with time of samples immersion in solutions, the EIS and OCP tests were performed during 74 and 110 h, respectively. The electrochemical tests were repeated for three samples for the reliability and reproducibility. The errors for calculated values of the main parameters of equivalent electrical circuits (EEC) (such as CPE and R) have not exceeded 5 %.

2.3. Immersion experiments, weight loss measurements and cross-section preparation

Immersion experiments in MEM and 0.83 % NaCl solution were performed for a period of up to 30 days. The size of the samples was 15 mm × 20 mm × 1.5 mm and the solution volume was equal to 1000 mL. The electrolyte was without contact with air. The experiment was performed at room temperature.

At the end of 30 days immersion test, the samples were etched with the chromic acid (200 g L⁻¹ CrO₃ + 10 g L⁻¹ AgNO₃) to remove the corrosion products for weight loss measurements. The corrosion rate (mm year⁻¹) was calculated in accordance with the earlier works [47,48].

After 8, 24, 40, 64 h and 30 days immersion of the samples in the MEM, the cross-section was prepared by means of Tegramin-25 system (Struers, Denmark). The plates were imbedded into ViaFix acrylic resin. After preliminary treating with SiC sandpapers, the sample was ground with the MD-Largo disk using 9 μm diamond suspension, and then polished with MD-Mol and MD-Nap disks using 3 and 1 μm diamond suspensions, respectively. DP-Lubricant brown was used as cooling and lubricating liquid for grinding and polishing. After polishing, the samples were washed with deionized water, degreased with ethanol and air-dried. All materials for grinding and polishing were products of Struers (Denmark).

2.4. Corrosion product characterization

At the end of the immersion experiments, the samples were removed from the solution, rinsed with deionized water, and dried in air. Raman spectroscopy was used to study the coating layers and corrosion products formed after 30 days of the alloy exposure to MEM. Raman spectra and images were obtained using confocal micro-Raman spectrometer alpha 500 (WITec, Ulm, Germany), and preprocessed with WITec Control/Project Plus 2.1 software. Raman spectra of corrosion film formed after sample immersion in corrosive solution were recorded between 300 and 4000 cm⁻¹ using 532 nm laser wavelength with a power of 20 mW. A 10 × objective (Zeiss EC “Epiplan” DIC, Germany) with a numerical aperture of 0.25 and 9.3 mm working distance was used to image the sample. The Raman spectra were collected from the area 250 × 250 μm. This data map contained 250 × 250 Raman spectra. The integration time used to obtain Raman spectrum was equal to 0.5 s. The average typical Raman spectrum is presented in this work. Background subtraction, baseline correction and peak deconvolution for obtained Raman spectra were done by means of Origin software.

The obtained cross-sections of the samples after 8, 24, 40, 64 h and 30 days immersion in MEM were used to study the morphology evolution of the corrosion film as well as element distribution in the formed surface layers by means of Zeiss EVO 40 scanning electron microscope (Carl Zeiss Group, Germany). SEM-images of the cross-section surface were obtained at an accelerating voltage of 20 kV. The SEM was equipped with Silicon Drift Detector X-Max^N 80 (Oxford Instruments NanoAnalysis, USA). The elements distribution over the cross-section surface of corrosion film was obtained by means of Energy Dispersive X-Ray (EDX) Analysis. The EDX measurements were performed by means of AZtec 3.0 SP2 software (Oxford Instruments NanoAnalysis, USA). The nanoscale chromium layers were deposited on the specimen surfaces to decrease image distortion related to a non-conductive layer charging. The Cr peaks were excluded during the EDX analysis.

3. Results and discussion

3.1. Electrochemical analysis of the MA8 Mg alloy behaviour in MEM and 0.83 % NaCl solutions

In order to study and compare the electrochemical behaviour of the MA8 Mg alloy samples in MEM and NaCl solutions, PDP, OCP and EIS tests were done. Fig. 1 depicts PDP curves for the samples in MEM and 0.83 % NaCl solutions. Values of corrosion current density calculated from the experimental data (after 1 h of the sample exposure) by means of LEV method ($I_{C\text{ LEV}}$) and using intersection of the straight line parallel to Y-axis through E_C with the cathodic Tafel extrapolation curve (I_C) for the sample in MEM were $9.2\ \mu\text{A cm}^{-2}$ and $7.3\ \mu\text{A cm}^{-2}$, respectively, which are two times lower than those for the specimen in NaCl solution ($22\ \mu\text{A cm}^{-2}$ and $18\ \mu\text{A cm}^{-2}$) (Table 1). It should be noted that values of current density calculated using two different methods were close to each other.

Values of the corrosion rate calculated from PDP curves (using I_C) [49,50] for Mg alloy in MEM and 0.83 % NaCl solutions were $0.17\ \text{mm year}^{-1}$ and $0.41\ \text{mm year}^{-1}$. The long-term steady-state corrosion rates evaluated from weight loss measurements after 30 days immersion were lower than those established from electrochemical measurements: $0.15 \pm 0.02\ \text{mm year}^{-1}$ ($0.07 \pm 0.01\ \text{mg cm}^{-2}\ \text{day}^{-1}$) for the sample in MEM and $0.19 \pm 0.02\ \text{mm year}^{-1}$ ($0.09 \pm 0.01\ \text{mg cm}^{-2}\ \text{day}^{-1}$) for the specimen in NaCl solution. These differences are related to the features of Mg corrosion as well as to the different times of the corrosion rate evaluation. The corrosion rate calculated from PDP is an instantaneous measurement, which is usually performed soon after the sample immersed in the solution. At the same time, the weight loss test provides the corrosion rate over the whole duration of immersion test [51]. However, in our work, both rates calculated from two independent methods have comparable values. It should be noted that this work was carried out *in vitro*, however, the degradation rate of the Mg samples studied *in vivo* was lower than in the tests performed in laboratory conditions as it was shown in the previous studies [52–57].

The data, presented in Table 1 indicated the lower corrosion activity of the sample in MEM in comparison to the one in NaCl solution. This result showed higher protective properties of the corrosion product film, formed in MEM than in NaCl medium. The sample immersed in MEM has lower corrosion potential ($E_C = -1.67\ \text{V}$) in comparison with one in NaCl medium ($E_C = -1.57\ \text{V}$) (Table 1), which is connected with different chemical reactions occurred on the material surface. Anodic and cathodic Tafel slopes, β_a and β_c , determined from PDP curves using LEV method are also presented in Table 1.

The evolution of the open circuit potential of the samples immersed in MEM (the lower curve) and in NaCl solution (the higher curve) is shown in Fig.2. The potential for the sample in MEM increased with time, whereas for the specimen in NaCl solution it was nearly constant during one hour.

The EIS was used to study the medium influence on the corrosion activity of the MA8 Mg alloy samples. The evolution of the EIS spectra versus time of the sample exposure to the NaCl solution and MEM is presented in Fig. 3 and Fig. 4, respectively. Impedance spectra (Figs. 3, 4) contain experimental data (symbols) and theoretical fitting curves (lines), which simulate the experimental results by means of equivalent electrical circuits (Figs. 3c, 4c). Results of the fitting of the experimental EIS data (Figs. 3, 4) are presented in Tables 2 and 3. EIS spectra for the sample immersed in MEM contain two time constants and there are first signs of the third time constant at low frequencies. This means that additional

dense layer of corrosion products develops on top of $\text{Mg}(\text{OH})_2$. This layer possesses higher protective ability, which decreased the degradation process of the magnesium alloy in MEM, compared to that in NaCl solution. The appearance of the third time constant at low frequencies can also be a result of the corrosion activity at the metal surface [58,59].

The evolution of the values of the impedance modulus measured at the lowest frequency ($|Z|_{f=0.1\text{Hz}}$) is presented in Fig. 5. Impedance modulus for the sample in MEM gradually increased during the 54 h from $5.5 \times 10^3 \Omega \text{ cm}^2$ up to $5.8 \times 10^4 \Omega \text{ cm}^2$ and then decreased dramatically down to $1.0 \times 10^3 \Omega \text{ cm}^2$. This is related to the gradual formation of the layer of corrosion products (up to 54 h) and its breakdown (after 54 h). Impedance modulus for the specimen in NaCl solution barely changed during 74 h. There are periods of impedance growth and drop with the maximum value $8.2 \times 10^3 \Omega \text{ cm}^2$ after 53 h of the exposure.

The impedance modulus for the sample immersed in MEM was higher than one in NaCl solution during most of the experimental time (Fig. 5).

In this study, we used the CPE (*CPE* – Constant Phase Element) in equivalent electrical circuit as a result of high level of heterogeneity of the studied system [42,47,60–62]. Impedance of the CPE was calculated in accordance with the equation:

$$Z_{CPE} = 1/[Q(j\omega)^n], \quad (2)$$

where ω is the radial frequency ($\omega = 2\pi f$), j is an imaginary unit, n is the exponential factor ($-1 \leq n \leq 1$), and Q is the CPE coefficient or CPE constant [63,64]. Impedance spectra for the samples in NaCl and MEM solutions were fitted with high accuracy ($\chi^2 = 1 \times 10^{-4}$).

Analysis of the spectra in Figs. 3a,b shows the presence of one time constant, which is corresponded to partially protective oxide-hydroxide corrosion film formed on Mg surface in NaCl solution. EEC, which was used for fitting of EIS data (Fig. 3c) consists of the solution resistance (R_s) in series with parallel constant phase element (CPE_1) and resistor (R_1), which applied to describe the capacitive and resistive behaviour of the corrosion layer, respectively.

The EIS spectra in MEM have two time constants (Fig. 4b). In the previous studies [65] the double layered structure of the corrosion film formed in Dulbecco's Modified Eagle's Medium was established. Therefore, for MA8 Mg alloy in MEM the EEC with a serial-parallel connection of two R - CPE -circuits (Fig. 4c) was used [9,36,60,66–75]. The elements in the EEC for MA8 Mg alloy in MEM (Fig. 4c) include the solution resistance (R_s), and two consecutive groups of paralleled combination of constant phase element (CPE_1 and CPE_2) and resistor (R_1 and R_2), which assigned to capacitive and resistive parameters of the outer and inner corrosion layer, respectively.

Constant phase element coefficient, Q , is similar to the interfacial capacitance [76]. Capacitance depends on the thickness of the oxide film and an increase in film thickness results in lowering of Q value [77]. This indicates that evolution of Q can be applied for evaluation of corrosion film condition during immersion in solution [8,63]. Authors of the work [78] also used Q to calculate the oxide film thickness. At the same time, besides Q evolution, the change of n can also strongly influence the computation accuracy of oxide layer thickness. Therefore, we have calculated the effective capacitance (C). The way of conversion a CPE parameter to C has been proposed by Brug et. al. [79], Hsu and Mansfeld [80],

Hirschorn et al. [81] and was discussed by many researcher groups [81–85]. However, in this work to calculate the effective capacitance of the corrosion product layers Brug formula or Hirschorn formula (3) was applied [79,81]. This equation can be used in case of a normal time-constant distribution [86] and was suggested for calculation of film capacitance [81].

$$C = Q^{\frac{1}{n}}(R_f^{\frac{1-n}{n}}), \quad (3)$$

where C is a corrosion film capacitance expressed in ($F \cdot cm^2$), R_f is the resistance of a film.

The evolution of the C and R calculated parameters with time of samples immersion (Tables 2, 3) in NaCl solution and in MEM is presented in Figs. 6, 7, respectively. For the specimen in NaCl solution after the first few hours the general tendency of C_1 (capacitance of the corrosion film) decrease and R_1 growth was established. n changes in the range from 0.8 up to 0.9, which indicates the low level of heterogeneity of the oxide film. The trends of these parameters indicated the formation of the barely protective film of the $Mg(OH)_2$ corrosion product.

The trend to the decreasing the capacitance of outer and inner corrosion layers (C_1) and (C_2), respectively for the sample in MEM during 54 h of exposure indicates the increase of the inner and outer sublayer thicknesses (Fig. 7) of the film. The heterogeneity of the studied surface is shown by parameter n , which is less than 1 in Tables 2, 3. It should be noted that exponential factors of CPE for samples in NaCl solution and MEM (Tables 2, 3) did not change sufficiently to make an essential correction in the interpretation of coating thickness evolution trend using analysis of the parameter Q . n of CPE_1 and CPE_2 for the sample in MEM changes in the range from 0.8 up to 1.0, and from 0.7 up to 0.8, respectively, indicating the capacitive behavior of CPE . Analysis of C and Q as functions of time indicates their similar trend of changing (Tables 2, 3). Therefore, the evolution of C and Q is the result of the corrosion film formation process, which slows down the degradation rate. After 54 h, parameters C and Q start to increase continuously, which is a result of corrosion film destruction. Evolution of the outer and inner layer resistance (R_1) and (R_2) (Table 3, Fig. 7) during specimen immersion also confirms the increase of the corrosion film protection as a result of decrease of the total number of defects over the surface (during 54 h) and breakdown of the protective film after 54 h. All the calculated EEC parameters (Table 3, Fig. 7) and impedance modulus measured at the lowest frequency (Fig. 5, the curve for MEM) are obeyed the same tendency with 54 h as the film breakdown time. Optical images of the sample surface obtained during its exposure to MEM confirm the surface film degradation process after 54 h (Fig. 8).

In order to study the potential evolution for the samples in NaCl solution and in MEM the OCP was recorded during 110 h of specimen immersion. Analysis of the results presented in Fig. 9 indicated that while the potential for the sample in NaCl with several periods of growth practically did not change with the average value of $-1.60 V \pm 0.03V$, the OCP for the specimen in MEM seriously changed during experimental time. Just like impedance modulus evolution (Fig. 5), the OCP of the alloy in MEM continuously increased (up to $-1.44 V$) during the 54 h and then decreased (down to $-1.95 V$) for the next 20 h. OCP started to increase again after 74 h, this indicates that the process of film formation and degradation is dynamic. These periods of corrosion film growth and breakdown continue until the

components of the MEM, especially HPO_4^{2-} , HCO_3^- and Ca^{2+} are depleted. After that, the Mg corrosion continues following the general degradation trend as in simple NaCl solution.

It should be noted that according to the fitting results of EIS data (Tables 2, 3), total resistance ($R_1 + R_2$) of the film formed in MEM was equal to $69.3 \text{ k}\Omega \text{ cm}^2$ after 54 h, which is nine times higher than resistance of the film formed in NaCl solution ($7.7 \text{ k}\Omega \text{ cm}^2$ after 53 h). This indicates the higher protective properties of the deposited film formed on the MA8 Mg alloy surface in MEM, which inhibits degradation rate, as compared to the film formed in NaCl solution. These findings are similar to work [6] where additional time constant in EIS spectra gradually revealed itself as commercially pure Mg was immersed in simulated body fluid. That was explained by gradual growth of partially protective layer of magnesium-substituted hydroxyapatite.

3.2. Chemical composition of the film formed on MA8 Mg alloy in MEM

Since the Raman spectroscopy is an appropriate technique to study metal surfaces [4], in this work it was used to study the particular corrosion products formed after 30 days of Mg alloy immersion in minimum essential medium. The Raman spectrum was acquired from the limited area presented in Fig. 10a. This spectrum is displayed in Fig. 10b. Sharp peaks at 417 and 3788 cm^{-1} can be attributed to the (O-H) stretching vibrations in the crystal structure of $\text{Mg}(\text{OH})_2$ [87]. The broad band in the wave number range $3500\text{--}2800 \text{ cm}^{-1}$ corresponding to stretching vibrations of hydroxyl ($-\text{OH}$) group is observed (with the maximum at 3085 cm^{-1}) [88–90]. The presence of Raman bands at 405 cm^{-1} (ν_2 bending vibrations), 594 cm^{-1} (ν_4 out-of-plane bending vibrations) and 1084 cm^{-1} (ν_3 antisymmetric stretching vibrations) can be assigned to the HPO_4^{2-} and PO_4^{3-} groups [91]. The Raman band around 960 cm^{-1} corresponds to the symmetric stretching mode of ν_1 (P-O) of HPO_4^{2-} group. After 30 days of immersion in MEM, the formation of a well-defined Raman band at 960 cm^{-1} confirms the hydroxyapatite formation. That is related to the symmetric stretching (ν_1) mode of PO_4^{3-} group of apatite phase [91–93].

Due to the presence of amino acids like glutamine in MEM, which has an additional uncharged amino group and is very sensitive in the $1500\text{--}1800 \text{ cm}^{-1}$ region, the Raman spectrum has wide band, where extensive coupling is observed among the $\nu \text{ COO}^-$, $\delta \text{ NH}_3^+$, $\nu \text{ C=O}$ and $\delta \text{ NH}_2$ vibrations [94–96]. The NH^+ bending vibrations are detected at $\sim 1640 \text{ cm}^{-1}$, the COO^- stretching vibrations at $\sim 1600 \text{ cm}^{-1}$ [94–96] and the band at 1705 cm^{-1} can be related to $\nu \text{ C=O}$ [88,90,97].

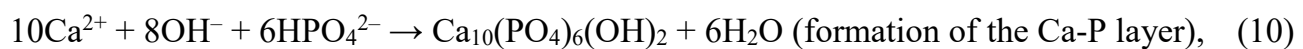
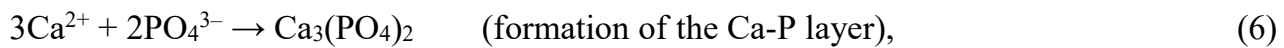
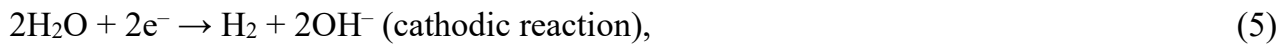
The $900\text{--}1100 \text{ cm}^{-1}$ spectral region can be characterized by bands associated with several C–C and C–N stretching vibrations, ν (C–C) and ν (C–N). The band detected at 1135 cm^{-1} can be attributed to NH_3^+ . The band observed at 1242 cm^{-1} is assigned to torsion of CH_2 , $\tau \text{ CH}_2$. Bands in the $1300\text{--}1375 \text{ cm}^{-1}$ region are related to the deformation vibrations of CH unit, $\delta \text{ CH}$ [98]. The band observed at 1476 cm^{-1} is pertained to the stretching vibrations of C–N [98].

Analysis of the SEM-EDX maps presented in Fig. 11 shows the bilayer structure of the corrosion product film formed in MEM. The inner layer consists predominantly from Mg and O (Figs. 11c, 11d) and the outer one from Ca, P, C and O (Figs. 11d, 11e, 11f, 11g). The thickness of the film was $15\text{--}25 \mu\text{m}$. The combined results of the Raman spectra (Fig. 10) and SEM-EDX maps indicate that $\text{MgO-Mg}(\text{OH})_2$ compounds formed the inner sublayer of the corrosion product film obtained in MEM, whereas

$\text{Ca}_x(\text{H}_y\text{PO}_4)_z$ formed the outer one. Among calcium-phosphorous compounds, hydroxyapatite one ($\text{Ca}_{10}(\text{PO}_4)_6(\text{OH})_2$) could also be formed in the outer layer according to the Raman data. Formation of hydroxyapatite or hydroxyapatite-like product (magnesium-substituted hydroxyapatite) as a component of corrosion product film in similar to this work condition was confirmed by different methods in [5,65,99–104]. The outer layer also contains adsorbed organic substances and possibly MgCO_3 , that is shown by the presence of corresponded functional groups (CH_2 , CN , CO , NH_2) (Fig. 10b) and high carbon concentration (Fig. 11b, 11e). According to the SEM-EDX map (Fig. 11b) the interface between inner and outer layer contains cerium. This is related to the dissolution of the magnesium matrix and intermetallic phases of the MA8 alloy, containing Ce e.g. Mg_9Ce [48].

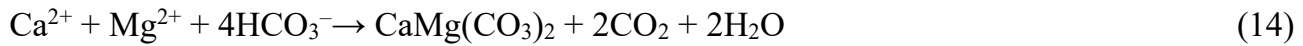
3.3 Corrosion mechanism of the MA8 Mg alloy in MEM

In order to study the mechanism of the film formation on the MA8 Mg alloy in MEM the cross-sections of the samples after 8, 24, 40 and 64 h of exposure were made in accordance with key point time determined from OCP and EIS data (Figs. 4, 5, 7, 9). According to the abovementioned results, during the first 54 h film formation took place and after that a breakdown occurred. SEM-EDX maps of the formed surface layer were obtained to study the stages of the film development, (Fig. 12). The sample exposure to MEM during 40 h (Figs. 12a-12c) leads to the formation of the thin film, which mainly consists of Ca, P, O containing compounds (Figs. 12(c1-c3)). This is the first stage of the samples corrosion process in MEM. Based on the obtained results the schematic illustration of the possible corrosion mechanism of magnesium alloy in the MEM is presented in Fig. 13. The first stage of the corrosion is shown in Fig. 13a, where the following chemical reactions can occur:



In accordance with our previous work [23], the local pH measured on the surface of the MA8 Mg alloy in MEM was in the range of 7.5 – 8.5. It was concluded that formation of protective magnesium-substituted hydroxyapatite layer stabilizes the local pH of MEM near 8.0 and inhibits the magnesium corrosion. Thereby, to correlate the reactions possible on the Mg alloy surface in MEM with local pH measured in [23] the diagram made using Hydra/Medusa[®] [105] software is presented in Fig. 14. This diagram shows the logarithm of concentration as a function of pH for the studied system. Analysis of results shows that $\text{Ca}_5(\text{PO}_4)_3\text{OH}$, $\text{CaMg}(\text{CO}_3)_2$, MgCO_3 , and CaCO_3 are stable in the range of pH 7–9. Therefore, the most probable reactions that occurred on the Mg alloy surface in MEM at the measured pH values are (10, 12-14).





Formation of the mixed phases of magnesium-calcium phosphate-carbonate is also possible [100,101], however, these phases are often amorphous, of varying chemical composition and with unknown solubility products.

The inorganic ions and their concentration taken to set up the system presented in Fig. 14, are the same as in MEM. It should be noted that during magnesium exposure to MEM the concentration of Mg^{2+} will increase, especially near the specimen surface that makes some variations in Fig. 14 (e.g. $\text{Mg}(\text{OH})_2$ formation (reaction (11)) can be realized at lower pH than in Fig. 14). This result confirms the thermodynamic possibility of the hydroxyapatite formation in the composition of corrosion products.

As immersion time elapses, the Ca-P layer started to grow and crack, and therefore the corrosive medium penetrates to the alloy substrate. This leads to the material destruction, appearance of the corroded lagoons, which are filled with magnesium hydroxide (Figs. 12d, 12(d1-d4)), formed according to the (11). This is the second stage of the corrosion process, which is presented in Fig. 13b.

The total corrosion layer thickness increased due to the intensive corrosion under the Ca-P layer with the formation of $\text{Mg}(\text{OH})_2$ inner sublayer (Figs. 11a, 12d). At the same time, the film breakdown at 54 h can be a result of one filiform event, which is not reflected in the general appearance of the sample. Therefore, it is difficult to find differences between the first and second stages. Probably these stages (formation of Ca-P outer layer and $\text{Mg}(\text{OH})_2$ inner sublayer) occurred simultaneously. Moreover, according to the Hydra/Medusa diagram and results of the previous work [23] $\text{Mg}(\text{OH})_2$ is not the main corrosion product. Thereby, the corrosion layer in Figs. 12d, 12(d1-d4) can consist of hydroxyapatite (Ca-P layer) depleted in Mg and rich in O.

Comparison of the corrosion film after 30 days (Fig. 11a) and after 64 h (Fig. 12d) also indicated that during long immersion of the sample in MEM the thickness of the outer layer increased due to sorption on the surface remaining Ca-P compounds and organic substances (like $\text{C}_5\text{H}_{10}\text{N}_2\text{O}_3$ – glutamine, $\text{C}_6\text{H}_{14}\text{N}_4\text{O}_2$ – arginine, etc.), as well as due to precipitation of MgCO_3 , which is shown by the carbon presence in the top-most layer of the film (Fig. 11b). The scheme of the resulted corrosion film formed on the magnesium alloy surface is presented in Fig. 13c (the third stage of the Mg alloy corrosion in MEM).

Fig. 13 offers the schematic illustrations of possible processes occurring in MEM and on the specimen surface. However, the sequence of stages presented in Fig. 13 might be changed.

The obtained results indicated the lower corrosion activity of the MA8 Mg alloy in MEM than in 0.83 % NaCl solution. Nevertheless, in order to prolong the implant integrity, application of the protective biocompatible coatings is desirable. This is the objective of our future studies.

Conclusions

The comparative detailed analysis of the corrosion activity of the MA8 Mg alloy (intended as bioresorbable materials) in the mammalian cell culture medium (MEM) and in 0.83 wt. % NaCl established the following.

- 1) The higher protective properties of the corrosion film formed on the alloy surface exposed in MEM have been established using EIS, PDP and OCP tests. Corrosion current density (after 1 h of sample exposure) was two times lower for the sample immersed in MEM than that for the samples exposed to NaCl solution.
- 2) The distinct trends of the development of corrosion process on the MA8 Mg alloy in two media were established by fitting of the EIS experimental results using appropriate EECs. There were two periods of corrosion film evolution in MEM: the process of formation (up to 54 h) and breakdown (after 54 h), which were repeated until the components of the MEM were consumed. The maximum total resistance of the film formed in MEM was $69.3 \text{ k}\Omega \text{ cm}^2$ (after 54 h), which is nine times higher than for the film formed in NaCl solution ($7.7 \text{ k}\Omega \text{ cm}^2$).
- 3) The bilayer structure of the corrosion film formed in MEM on the MA8 Mg alloy surface was revealed according to the analysis of the SEM-EDX maps of the sample cross-sections. The combined results of the Raman data and SEM-EDX analysis indicated that MgO-Mg(OH)₂ compounds formed the inner sublayer of the corrosion film grown in MEM, whereas Ca_x(H_yPO₄)_z (including hydroxyapatite) formed the outer one. The top-most layer with high carbon concentration connected with MgCO₃ precipitation and sorption of the organic constituents of MEM on the material surface.
- 4) Possible corrosion mechanism for MA8 Mg alloy in the MEM, which revealed three stages of the corrosion film evolution, was proposed. Calcium and phosphorus containing products, including hydroxyapatite, are the main precipitates on the Mg alloy surface exposed to MEM.

Data availability

The raw/processed data required to reproduce these findings cannot be shared at this time as the data also forms part of an ongoing study.

Acknowledgements

This work was supported by the Grant of Russian Science Foundation (project no. 19-73-00078). The results of Raman spectroscopy were collected under the government assignments from Ministry of Science and Higher Education of the Russian Federation (project no. 0265-2019-0001).

References

- [1] E. Galvin, S. Jaiswal, C. Lally, B. MacDonald, B. Duffy, In Vitro Corrosion and Biological Assessment of Bioabsorbable WE43 Mg Alloy Specimens, *J. Manuf. Mater. Process.* 1 (2017) 8. doi:10.3390/jmmp1010008.
- [2] Q. Chen, G.A. Thouas, Metallic implant biomaterials, *Mater. Sci. Eng. R Reports.* 87 (2015) 1–57. doi:10.1016/j.mser.2014.10.001.
- [3] F. Witte, J. Fischer, J. Nellesen, C. Vogt, J. Vogt, T. Donath, F. Beckmann, In vivo corrosion and corrosion protection of magnesium alloy LAE442☆, *Acta Biomater.* 6 (2010) 1792–1799. doi:10.1016/j.actbio.2009.10.012.
- [4] M. Esmaily, J.E. Svensson, S. Fajardo, N. Birbilis, G.S. Frankel, S. Virtanen, R. Arrabal, S. Thomas, L.G. Johansson, Fundamentals and advances in magnesium alloy corrosion, *Prog. Mater. Sci.* 89 (2017) 92–193. doi:10.1016/J.PMATSCI.2017.04.011.
- [5] S. V. Lamaka, J. Gonzalez, D. Mei, F. Feyerabend, R. Willumeit-Römer, M.L. Zheludkevich, Local pH and Its Evolution Near Mg Alloy Surfaces Exposed to Simulated Body Fluids, *Adv.*

- Mater. Interfaces. 5 (2018) 1800169. doi:10.1002/admi.201800169.
- [6] D. Mei, S. V. Lamaka, J. Gonzalez, F. Feyerabend, R. Willumeit-Römer, M.L. Zheludkevich, The role of individual components of simulated body fluid on the corrosion behavior of commercially pure Mg, *Corros. Sci.* 147 (2019) 81–93. doi:10.1016/j.corsci.2018.11.011.
- [7] X.-B. Chen, C. Li, D. Xu, Biodegradation of Mg-14Li alloy in simulated body fluid: A proof-of-concept study, *Bioact. Mater.* 3 (2018) 110–117. doi:10.1016/J.BIOACTMAT.2017.08.002.
- [8] G. Rondelli, P. Torricelli, M. Fini, R. Giardino, In vitro corrosion study by EIS of a nickel-free stainless steel for orthopaedic applications, *Biomaterials.* 26 (2005) 739–744. doi:10.1016/J.BIOMATERIALS.2004.03.012.
- [9] H.R. Bakhsheshi-Rad, M. Abdollahi, E. Hamzah, A.F. Ismail, M. Bahmanpour, Modelling corrosion rate of biodegradable magnesium-based alloys: The case study of Mg-Zn-RE-xCa (x = 0, 0.5, 1.5, 3 and 6 wt%) alloys, *J. Alloys Compd.* 687 (2016) 630–642. doi:10.1016/J.JALLCOM.2016.06.149.
- [10] A. Witecka, A. Yamamoto, W. Świąszkowski, Influence of SaOS-2 cells on corrosion behavior of cast Mg-2.0Zn0.98Mn magnesium alloy, *Colloids Surfaces B Biointerfaces.* 150 (2017) 288–296. doi:10.1016/J.COLSURFB.2016.10.041.
- [11] C.L. Liu, Y.J. Wang, R.C. Zeng, X.M. Zhang, W.J. Huang, P.K. Chu, In vitro corrosion degradation behaviour of Mg–Ca alloy in the presence of albumin, *Corros. Sci.* 52 (2010) 3341–3347. doi:10.1016/J.CORSCI.2010.06.003.
- [12] J. Kim, H.M. Mousa, C.H. Park, C.S. Kim, Enhanced corrosion resistance and biocompatibility of AZ31 Mg alloy using PCL/ZnO NPs via electrospinning, *Appl. Surf. Sci.* 396 (2017) 249–258. doi:10.1016/J.APSUSC.2016.10.092.
- [13] A.C. Hänzi, I. Gerber, M. Schinhammer, J.F. Löffler, P.J. Uggowitzer, On the in vitro and in vivo degradation performance and biological response of new biodegradable Mg–Y–Zn alloys, *Acta Biomater.* 6 (2010) 1824–1833. doi:10.1016/J.ACTBIO.2009.10.008.
- [14] H.B. Yao, Y. Li, A.T.S. Wee, Passivity behavior of melt-spun Mg–Y Alloys, *Electrochim. Acta.* 48 (2003) 4197–4204. doi:10.1016/S0013-4686(03)00605-4.
- [15] J. Niu, G. Yuan, Y. Liao, L. Mao, J. Zhang, Y. Wang, F. Huang, Y. Jiang, Y. He, W. Ding, Enhanced biocorrosion resistance and biocompatibility of degradable Mg–Nd–Zn–Zr alloy by brushite coating, *Mater. Sci. Eng. C.* 33 (2013) 4833–4841. doi:10.1016/J.MSEC.2013.08.008.
- [16] Y. Shangguan, L. Sun, P. Wan, L. Tan, C. Wang, X. Fan, L. Qin, K. Yang, Comparison study of different coatings on degradation performance and cell response of Mg-Sr alloy, *Mater. Sci. Eng. C.* 69 (2016) 95–107. doi:10.1016/J.MSEC.2016.06.073.
- [17] B.M. Wilke, L. Zhang, W. Li, C. Ning, C. Chen, Y. Gu, Corrosion performance of MAO coatings on AZ31 Mg alloy in simulated body fluid vs. Earle’s Balance Salt Solution, *Appl. Surf. Sci.* 363 (2016) 328–337. doi:10.1016/J.APSUSC.2015.12.026.
- [18] A. Yamamoto, S. Hiromoto, Effect of inorganic salts, amino acids and proteins on the degradation of pure magnesium in vitro, *Mater. Sci. Eng. C.* 29 (2009) 1559–1568. doi:10.1016/j.msec.2008.12.015.
- [19] S. Virtanen, Biodegradable Mg and Mg alloys: Corrosion and biocompatibility, *Mater. Sci. Eng. B.* 176 (2011) 1600–1608. doi:10.1016/J.MSEB.2011.05.028.
- [20] S. Höhn, S. Virtanen, A.R. Boccaccini, Protein adsorption on magnesium and its alloys: A review, *Appl. Surf. Sci.* 464 (2019) 212–219. doi:10.1016/J.APSUSC.2018.08.173.
- [21] M.B. Kannan, R.K.S. Raman, In vitro degradation and mechanical integrity of calcium-containing magnesium alloys in modified-simulated body fluid, *Biomaterials.* 29 (2008) 2306–2314. doi:10.1016/J.BIOMATERIALS.2008.02.003.
- [22] L. Yang, E. Zhang, Biocorrosion behavior of magnesium alloy in different simulated fluids for biomedical application, *Mater. Sci. Eng. C.* 29 (2009) 1691–1696. doi:10.1016/J.MSEC.2009.01.014.
- [23] A.S. Gnedenkov, D. Mei, S.V. Lamaka, S.L. Sinebryukhov, D.V. Mashtalyar, I.E. Vyaliy, S.V. Zheludkevich, M.L. Gnedenkov, Localized currents and pH distribution studied during corrosion

- of MA8 Mg alloy in the cell culture medium, *Corros. Sci.* (2020) Submitted to Journal.
- [24] S.V. Gnedenkov, S.L. Sinebryukhov, D.V. Mashtalyar, I.M. Imshinetskiy, A.S. Gnedenkov, A.V. Samokhin, Y.V. Tsvetkov, Protective composite coatings obtained by plasma electrolytic oxidation on magnesium alloy MA8, *Vacuum*. 120 (2015) 107–114. doi:10.1016/j.vacuum.2015.02.004.
- [25] A.S. Gnedenkov, S.L. Sinebryukhov, D. V. Mashtalyar, S. V. Gnedenkov, Inhibitor-Containing Composite Coatings on Mg Alloys: Corrosion Mechanism and Self-Healing Protection, *Solid State Phenom.* 245 (2016) 89–96. doi:10.4028/www.scientific.net/SSP.245.89.
- [26] A.S. Gnedenkov, S.L. Sinebryukhov, D.V. Mashtalyar, S.V. Gnedenkov, Features of the magnesium alloys corrosion in the chloride-containing media, *Solid State Phenom.* 213 (2014) 143–148. doi:10.4028/www.scientific.net/SSP.213.143.
- [27] A.S. Gnedenkov, S.L. Sinebryukhov, D. V. Mashtalyar, S. V. Gnedenkov, Microscale morphology and properties of the PEO-coating surface, in: *Phys. Procedia*, 2012: pp. 98–101. doi:10.1016/j.phpro.2012.01.025.
- [28] A.S. Gnedenkov, S.L. Sinebryukhov, D.V. Mashtalyar, S.V. Gnedenkov, Localized corrosion of the Mg alloys with inhibitor-containing coatings: SVET and SIET studies, *Corros. Sci.* 102 (2016) 269–278. doi:10.1016/j.corsci.2015.10.015.
- [29] D.V. Mashtalyar, S.V. Gnedenkov, S.L. Sinebryukhov, I.M. Imshinetskiy, A.S. Gnedenkov, V.M. Bouznik, Composite coatings formed using plasma electrolytic oxidation and fluoroparaffin materials, *J. Alloys Compd.* 767 (2018) 353–360. doi:10.1016/j.jallcom.2018.07.085.
- [30] G.L. Makar, J. Kruger, Corrosion of magnesium, *Int. Mater. Rev.* 38 (1993) 138–153. doi:10.1179/imr.1993.38.3.138.
- [31] D. Eaves, G. Williams, H.N. McMurray, Inhibition of self-corrosion in magnesium by poisoning hydrogen recombination on iron impurities, *Electrochim. Acta.* 79 (2012) 1–7. doi:10.1016/j.electacta.2012.05.148.
- [32] D.S. Gandel, M.A. Easton, M.A. Gibson, N. Birbilis, CALPHAD simulation of the Mg-(Mn, Zr)-Fe system and experimental comparison with as-cast alloy microstructures as relevant to impurity driven corrosion of Mg-alloys, *Mater. Chem. Phys.* 143 (2014) 1082–1091. doi:10.1016/j.matchemphys.2013.11.008.
- [33] K. Gusieva, C.H.J. Davies, J.R. Scully, N. Birbilis, Corrosion of magnesium alloys: the role of alloying, *Int. Mater. Rev.* 60 (2015) 169–194. doi:10.1179/1743280414Y.0000000046.
- [34] E.F. Volkova, Effect of iron impurity on the phase composition, structure and properties of magnesium alloys containing manganese and aluminum, *Met. Sci. Heat Treat.* 59 (2017) 154–160. doi:10.1007/s11041-017-0120-2.
- [35] K. Watcharat, W. Korchunjit, S. Buranasinsup, J. Taylor, P. Ritruethai, T. Wongtawan, MEM α Promotes Cell Proliferation and Expression of Bone Marrow Derived Equine Mesenchymal Stem Cell Gene Markers but Depresses Differentiation Gene Markers, *J. Equine Vet. Sci.* 50 (2017) 8–14. doi:10.1016/j.jevs.2016.10.017.
- [36] J. Wang, Y. Jang, G. Wan, V. Giridharan, G.-L. Song, Z. Xu, Y. Koo, P. Qi, J. Sankar, N. Huang, Y. Yun, Flow-induced corrosion of absorbable magnesium alloy: In-situ and real-time electrochemical study, *Corros. Sci.* 104 (2016) 277–289. doi:10.1016/J.CORSCI.2015.12.020.
- [37] Thermo Fisher Scientific, Inc. US. <https://www.thermofisher.com/order/catalog/product/61100103#/61100103> (accessed January 17, 2020).
- [38] ASTM G5-14, Standard Reference Test Method for Making Potentiodynamic Anodic Polarization Measurements, ASTM International, West Conshohocken, PA, 2014.
- [39] R. Bertolini, S. Bruschi, A. Ghiotti, L. Pezzato, M. Dabalà, Large strain extrusion machining of magnesium alloys for biomedical applications, *Procedia CIRP.* 71 (2018) 105–110. doi:10.1016/j.procir.2018.05.080.
- [40] S. Bruschi, R. Bertolini, A. Ghiotti, E. Savio, W. Guo, R. Shivpuri, Machining-induced surface transformations of magnesium alloys to enhance corrosion resistance in human-like environment,

- CIRP Ann. 67 (2018) 579–582. doi:10.1016/j.cirp.2018.04.040.
- [41] Z. Shi, A. Atrens, An innovative specimen configuration for the study of Mg corrosion, *Corros. Sci.* 53 (2011) 226–246. <https://www.sciencedirect.com/science/article/pii/S0010938X10004476> (accessed October 12, 2016).
- [42] F. Cao, Z. Shi, J. Hofstetter, P.J. Uggowitzer, G. Song, M. Liu, A. Atrens, Corrosion of ultra-high-purity Mg in 3.5% NaCl solution saturated with Mg(OH)₂, *Corros. Sci.* 75 (2013) 78–99. doi:10.1016/j.corsci.2013.05.018.
- [43] Y. Chen, Y. Yang, T. Zhang, W. Zhang, FuhuiWang, X. Lu, C. Blawert, M.L. Zheludkevich, Interaction effect between different constituents in silicate-containing electrolyte on PEO coatings on Mg alloy, *Surf. Coatings Technol.* 307 (2016) 825–836. doi:10.1016/j.surfcoat.2016.09.031.
- [44] G. Yoganandan, K. Pradeep Premkumar, J.N. Balaraju, Evaluation of corrosion resistance and self-healing behavior of zirconium-cerium conversion coating developed on AA2024 alloy, *Surf. Coatings Technol.* 270 (2015) 249–258. doi:10.1016/j.surfcoat.2015.02.049.
- [45] E. McCafferty, Validation of corrosion rates measured by the Tafel extrapolation method, *Corros. Sci.* 47 (2005) 3202–3215. doi:10.1016/j.corsci.2005.05.046.
- [46] R.L. LeRoy, Evaluation of Corrosion Rates from Nonlinear Polarization Data, *J. Electrochem. Soc.* 124 (1977) 1006–1012. doi:10.1149/1.2133470.
- [47] A.S. Gnedenkoy, S.L. Sinebryukhov, D.V. Mashtalyar, S.V. Gnedenkoy, Protective properties of inhibitor-containing composite coatings on a Mg alloy, *Corros. Sci.* 102 (2016) 348–354. doi:10.1016/j.corsci.2015.10.026.
- [48] A.S. Gnedenkoy, S.L. Sinebryukhov, D.V. Mashtalyar, S.V. Gnedenkoy, Features of the corrosion processes development at the magnesium alloys surface, *Surf. Coatings Technol.* 225 (2013) 112–118. doi:10.1016/j.surfcoat.2013.03.023.
- [49] Z. Shi, M. Liu, A. Atrens, Measurement of the corrosion rate of magnesium alloys using Tafel extrapolation, *Corros. Sci.* 52 (2010) 579–588. doi:10.1016/J.CORSCI.2009.10.016.
- [50] A. Atrens, G.-L. Song, M. Liu, Z. Shi, F. Cao, M.S. Dargusch, Review of Recent Developments in the Field of Magnesium Corrosion, *Adv. Eng. Mater.* 17 (2015) 400–453. doi:10.1002/adem.201400434.
- [51] A. Atrens, G.-L. Song, F. Cao, Z. Shi, P.K. Bowen, Advances in Mg corrosion and research suggestions, *J. Magnes. Alloy.* 1 (2013) 177–200. doi:10.1016/J.JMA.2013.09.003.
- [52] A.H.M. Sanchez, B.J.C. Luthringer, F. Feyerabend, R. Willumeit, Mg and Mg alloys: How comparable are in vitro and in vivo corrosion rates? A review, *Acta Biomater.* 13 (2015) 16–31. doi:10.1016/j.actbio.2014.11.048.
- [53] J. Hofstetter, E. Martinelli, A.M. Weinberg, M. Becker, B. Mingler, P.J. Uggowitzer, J.F. Löffler, Assessing the degradation performance of ultrahigh-purity magnesium in vitro and in vivo, *Corros. Sci.* 91 (2015) 29–36. doi:10.1016/j.corsci.2014.09.008.
- [54] J. Niu, M. Xiong, X. Guan, J. Zhang, H. Huang, J. Pei, G. Yuan, The in vivo degradation and bone-implant interface of Mg-Nd-Zn-Zr alloy screws: 18 months post-operation results, *Corros. Sci.* 113 (2016) 183–187. doi:10.1016/j.corsci.2016.10.009.
- [55] A. Myrissa, E. Martinelli, G. Szakács, L. Berger, J. Eichler, S.F. Fischerauer, C. Kleinhans, N. Hort, U. Schäfer, A.M. Weinberg, In vivo degradation of binary magnesium alloys - A long-term study, *BioNanoMaterials.* 17 (2016) 121–130. doi:10.1515/bnm-2016-0006.
- [56] J. Draxler, E. Martinelli, A.M. Weinberg, A. Zitek, J. Irrgeher, M. Meischel, S.E. Stanzl-Tschegg, B. Mingler, T. Prohaska, The potential of isotopically enriched magnesium to study bone implant degradation in vivo, *Acta Biomater.* 51 (2017) 526–536. doi:10.1016/j.actbio.2017.01.054.
- [57] E. Lukyanova, N. Anisimova, N. Martynenko, M. Kiselevsky, S. Dobatkin, Y. Estrin, Features of in vitro and in vivo behaviour of magnesium alloy WE43, *Mater. Lett.* 215 (2018) 308–311. doi:10.1016/j.matlet.2017.12.125.
- [58] B. Mingo, R. Arrabal, M. Mohedano, Y. Llamazares, E. Matykina, A. Yerokhin, A. Pardo, Influence of sealing post-treatments on the corrosion resistance of PEO coated AZ91 magnesium alloy, *Appl. Surf. Sci.* 433 (2018) 653–667. doi:10.1016/j.apsusc.2017.10.083.

- [59] J. Yang, X. Lu, C. Blawert, S. Di, M.L. Zheludkevich, Microstructure and corrosion behavior of Ca/P coatings prepared on magnesium by plasma electrolytic oxidation, *Surf. Coatings Technol.* 319 (2017) 359–369. doi:10.1016/j.surfcoat.2017.04.001.
- [60] S. Yagi, K. Kuwabara, Y. Fukuta, K. Kubota, E. Matsubara, Formation of self-repairing anodized film on ACM522 magnesium alloy by plasma electrolytic oxidation, *Corros. Sci.* 73 (2013) 188–195. doi:10.1016/J.CORSCI.2013.03.035.
- [61] S.V. Gnedenkov, S.L. Sinebryukhov, D.V. Mashtalyar, V.S. Egorkin, M.V. Sidorova, A.S. Gnedenkov, Composite polymer-containing protective coatings on magnesium alloy MA8, *Corros. Sci.* 85 (2014) 52–59. doi:10.1016/j.corsci.2014.03.035.
- [62] A.S. Gnedenkov, S.L. Sinebryukhov, D. V. Mashtalyar, I.E. Vyaliy, V.S. Egorkin, S. V. Gnedenkov, Corrosion of the welded aluminium alloy in 0.5 M NaCl solution. Part 2: Coating protection, *Materials (Basel)*. 11 (2018) 2177. doi:10.3390/ma11112177.
- [63] A. Jangde, S. Kumar, C. Blawert, Influence of glycerol on plasma electrolytic oxidation coatings evolution and on corrosion behaviour of coated AM50 magnesium alloy, *Corros. Sci.* (2019). doi:10.1016/j.corsci.2019.05.024.
- [64] R. Arrabal, A. Pardo, M.C. Merino, M. Mohedano, P. Casajús, E. Matykina, P. Skeldon, G.E. Thompson, Corrosion behaviour of a magnesium matrix composite with a silicate plasma electrolytic oxidation coating, *Corros. Sci.* 52 (2010) 3738–3749. doi:10.1016/j.corsci.2010.07.024.
- [65] V. Wagener, S. Virtanen, Protective layer formation on magnesium in cell culture medium, *Mater. Sci. Eng. C*. 63 (2016) 341–351. doi:10.1016/j.msec.2016.03.003.
- [66] C.S. Wu, Z. Zhang, F.H. Cao, L.J. Zhang, J.Q. Zhang, C.N. Cao, Study on the anodizing of AZ31 magnesium alloys in alkaline borate solutions, *Appl. Surf. Sci.* 253 (2007) 3893–3898. doi:10.1016/j.apsusc.2006.08.020.
- [67] L. Chang, L. Tian, W. Liu, X. Duan, Formation of dicalcium phosphate dihydrate on magnesium alloy by micro-arc oxidation coupled with hydrothermal treatment, *Corros. Sci.* 72 (2013) 118–124. doi:10.1016/J.CORSCI.2013.03.017.
- [68] T.S. Lim, H.S. Ryu, S.-H. Hong, Electrochemical corrosion properties of CeO₂-containing coatings on AZ31 magnesium alloys prepared by plasma electrolytic oxidation, *Corros. Sci.* 62 (2012) 104–111. doi:10.1016/J.CORSCI.2012.04.043.
- [69] S. V. Gnedenkov, O.A. Khrisanfova, S.L. Sinebryukhov, A. V. Puz, A.S. Gnedenkov, Composite protective coatings on nitinol surface, *Mater. Manuf. Process.* 23 (2008) 879–883. doi:10.1080/10426910802385117.
- [70] D. Snihirova, S. V. Lamaka, M.F. Montemor, “SMART” protective ability of water based epoxy coatings loaded with CaCO₃ microbeads impregnated with corrosion inhibitors applied on AA2024 substrates, *Electrochim. Acta.* 83 (2012) 439–447. doi:10.1016/J.ELECTACTA.2012.07.102.
- [71] H. Shi, E.-H. Han, S.V. Lamaka, M.L. Zheludkevich, F. Liu, M.G.S. Ferreira, Cerium cinnamate as an environmentally benign inhibitor pigment for epoxy coatings on AA 2024-T3, *Prog. Org. Coatings.* 77 (2014) 765–773. doi:10.1016/J.PORGCOAT.2014.01.003.
- [72] S.V. Lamaka, H.B. Xue, N.N.A.H. Meis, A.C.C. Esteves, M.G.S. Ferreira, Fault-tolerant hybrid epoxy-silane coating for corrosion protection of magnesium alloy AZ31, *Prog. Org. Coatings.* 80 (2015) 98–105. doi:10.1016/J.PORGCOAT.2014.11.024.
- [73] S.V. Gnedenkov, S.L. Sinebryukhov, D.V. Mashtalyar, K.V. Nadaraia, A.S. Gnedenkov, V.M. Bouzник, Composite fluoropolymer coatings on the MA8 magnesium alloy surface, *Corros. Sci.* 111 (2016) 175–185. doi:10.1016/j.corsci.2016.04.052.
- [74] S.L. Sinebryukhov, A.S. Gnedenkov, D.V. Mashtalyar, S.V. Gnedenkov, PEO-coating/substrate interface investigation by localised electrochemical impedance spectroscopy, *Surf. Coatings Technol.* 205 (2010) 1697–1701. doi:10.1016/j.surfcoat.2010.05.048.
- [75] S.V. Gnedenkov, S.L. Sinebryukhov, V.S. Egorkin, D.V. Mashtalyar, I.E. Vyaliy, K.V. Nadaraia, I.M. Imshinetskiy, A.I. Nikitin, E.P. Subbotin, A.S. Gnedenkov, Magnesium fabricated using

- additive technology: Specificity of corrosion and protection, *J. Alloys Compd.* 808 (2019) 151629. doi:10.1016/j.jallcom.2019.07.341.
- [76] M.E. Orazem, N. Pábre, B. Tribollet, Enhanced graphical representation of electrochemical impedance data, *J. Electrochem. Soc.* 153 (2006) B129–B136. doi:10.1149/1.2168377.
- [77] E. Matykina, R. Arrabal, M. Mohedano, A. Pardo, M.C. Merino, E. Rivero, Stability of plasma electrolytic oxidation coating on titanium in artificial saliva, *J. Mater. Sci. Mater. Med.* 24 (2013) 37–51. doi:10.1007/s10856-012-4787-z.
- [78] M. Mohedano, E. Matykina, R. Arrabal, A. Pardo, M.C. Merino, Metal release from ceramic coatings for dental implants, *Dent. Mater.* 30 (2014) e28–e40. doi:10.1016/j.dental.2013.12.011.
- [79] G.J. Brug, A.L.G. van den Eeden, M. Sluyters-Rehbach, J.H. Sluyters, The analysis of electrode impedances complicated by the presence of a constant phase element, *J. Electroanal. Chem.* 176 (1984) 275–295. doi:10.1016/S0022-0728(84)80324-1.
- [80] C.H. Hsu, F. Mansfeld, Concerning the conversion of the constant phase element parameter Y_0 into a capacitance, *Corrosion*. 57 (2001) 747–748. doi:10.5006/1.3280607.
- [81] B. Hirschorn, M.E. Orazem, B. Tribollet, V. Vivier, I. Frateur, M. Musiani, Determination of effective capacitance and film thickness from constant-phase-element parameters, *Electrochim. Acta*. 55 (2010) 6218–6227. doi:10.1016/j.electacta.2009.10.065.
- [82] C.M. Gore, J.O. White, E.D. Wachsman, V. Thangadurai, Effect of composition and microstructure on electrical properties and CO₂ stability of donor-doped, proton conducting BaCe_{1-(x+y)}Zr_xNb_yO₃, *J. Mater. Chem. A*. 2 (2014) 2363–2373. doi:10.1039/c3ta12668d.
- [83] P. Hjalmarsson, M. Søgaaard, M. Mogensen, Electrochemical behaviour of (La_{1-x}Sr_x)_sCo_{1-y}Ni_yO_{3-δ} as porous SOFC cathodes, *Solid State Ionics*. 180 (2009) 1395–1405. doi:10.1016/j.ssi.2009.08.007.
- [84] Q. Li, V. Thangadurai, A comparative 2 and 4-probe DC and 2-probe AC electrical conductivity of novel co-doped Ce_{0.9-x}RE_xMo_{0.1}O_{2.1-0.5x} (RE = Y, Sm, Gd; X = 0.2, 0.3), *J. Mater. Chem.* 20 (2010) 7970–7983. doi:10.1039/c0jm01324b.
- [85] Q. Li, V. Thangadurai, Synthesis, structure and electrical properties of Mo-doped CeO₂-Materials for SOFCs, *Fuel Cells*. 9 (2009) 684–698. doi:10.1002/fuce.200900044.
- [86] K.A. Yasakau, A. Kuznetsova, S. Kallip, M. Sarykevich, J. Tedim, M.G.S. Ferreira, M.L. Zheludkevich, A novel bilayer system comprising LDH conversion layer and sol-gel coating for active corrosion protection of AA2024, *Corros. Sci.* 143 (2018) 299–313. doi:10.1016/j.corsci.2018.08.039.
- [87] E.F. De Oliveira, Y. Hase, Infrared study and isotopic effect of magnesium hydroxide, *Vib. Spectrosc.* 25 (2001) 53–56. doi:10.1016/S0924-2031(00)00107-7.
- [88] B. Grabowska, M. Sitarz, E. Olejnik, K. Kaczmarek, FT-IR and FT-Raman studies of cross-linking processes with Ca²⁺ ions, glutaraldehyde and microwave radiation for polymer composition of poly(acrylic acid)/sodium salt of carboxymethyl starch – Part I, *Spectrochim. Acta Part A Mol. Biomol. Spectrosc.* 135 (2015) 529–535. doi:10.1016/J.SAA.2014.07.031.
- [89] I. Korybska-Sadło, G. Gil, P. Gunia, M. Horszowski, M. Sitarz, Raman and FTIR spectra of nephrites from the Złoty Stok and Jordanów Śląski (the Sudetes and Fore-Sudetic Block, SW Poland), *J. Mol. Struct.* 1166 (2018) 40–47. doi:10.1016/J.MOLSTRUC.2018.04.020.
- [90] B. Grabowska, M. Sitarz, E. Olejnik, K. Kaczmarek, B. Tyliczszak, FT-IR and FT-Raman studies of cross-linking processes with Ca²⁺ ions, glutaraldehyde and microwave radiation for polymer composition of poly(acrylic acid)/sodium salt of carboxymethyl starch – In moulding sands, Part II, *Spectrochim. Acta Part A Mol. Biomol. Spectrosc.* 151 (2015) 27–33. doi:10.1016/J.SAA.2015.06.084.
- [91] R.J. Kavitha, K. Ravichandran, T.S.N. Sankara Narayanan, Deposition of strontium phosphate coatings on magnesium by hydrothermal treatment: Characteristics, corrosion resistance and bioactivity, *J. Alloys Compd.* 745 (2018) 725–743. doi:10.1016/J.JALLCOM.2018.02.200.
- [92] J. Zhang, C. Dai, J. Wei, Z. Wen, S. Zhang, C. Chen, Degradable behavior and bioactivity of micro-arc oxidized AZ91D Mg alloy with calcium phosphate/chitosan composite coating in m-

- SBF, *Colloids Surfaces B Biointerfaces*. 111 (2013) 179–187. doi:10.1016/j.colsurfb.2013.05.040.
- [93] S.D. Huelin, H.R. Baker, E.F. Merschrod, K.M. Poduska, Phase-selective electroprecipitation of calcium phosphate thin films at physiological temperatures, *Cryst. Growth Des.* 6 (2006) 2634–2636. doi:10.1021/cg060410k.
- [94] T. Pazderka, V. Kopecký, Drop coating deposition Raman spectroscopy of proteinogenic amino acids compared with their solution and crystalline state, *Spectrochim. Acta Part A Mol. Biomol. Spectrosc.* 185 (2017) 207–216. doi:10.1016/J.SAA.2017.05.043.
- [95] A. Pawlukojć, K. Hołderna-Natkaniec, G. Bator, I. Natkaniec, INS, IR, RAMAN, ¹H NMR and DFT investigations on dynamical properties of l-asparagine, *Vib. Spectrosc.* 72 (2014) 1–7. doi:10.1016/J.VIBSPEC.2014.02.002.
- [96] J.T. López Navarrete, J. Casado, V. Hernández, F.J. Ramírez, Experimental and theoretical vibrational studies of the amino acid l-asparagine in solution, *J. Raman Spectrosc.* 28 (1997) 501–509. doi:10.1002/(SICI)1097-4555(199707)28:7<501::AID-JRS117>3.0.CO;2-B.
- [97] J.T. Edsall, Raman Spectra of Amino Acids and Related Compounds IV. Ionization of Di- and Tricarboxylic Acids, *J. Chem. Phys.* 5 (1937) 508–517. doi:10.1063/1.1750067.
- [98] G. Zhu, X. Zhu, Q. Fan, X. Wan, Raman spectra of amino acids and their aqueous solutions, *Spectrochim. Acta Part A Mol. Biomol. Spectrosc.* 78 (2011) 1187–1195. doi:10.1016/J.SAA.2010.12.079.
- [99] R. Rettig, S. Virtanen, Composition of corrosion layers on a magnesium rare-earth alloy in simulated body fluids, *J. Biomed. Mater. Res. Part A*. 88A (2009) 359–369. doi:10.1002/jbm.a.31887.
- [100] P.K. Bowen, J. Drelich, J. Goldman, Magnesium in the murine artery: Probing the products of corrosion, *Acta Biomater.* 10 (2014) 1475–1483. doi:10.1016/J.ACTBIO.2013.11.021.
- [101] P.K. Bowen, C.T. McNamara, O.P. Mills, J. Drelich, J. Goldman, FIB-TEM Study of Magnesium Corrosion Products after 14 Days in the Murine Artery, *ACS Biomater. Sci. Eng.* 1 (2015) 919–926. doi:10.1021/acsbiomaterials.5b00044.
- [102] H. Kuwahara, Y. Al-Abdullat, N. Mazaki, S. Tsutsumi, T. Aizawa, Precipitation of magnesium apatite on pure magnesium surface during immersing in Hank's solution, *Mater. Trans.* 42 (2001) 1317–1321. doi:10.2320/matertrans.42.1317.
- [103] S. Zhang, X. Zhang, C. Zhao, J. Li, Y. Song, C. Xie, H. Tao, Y. Zhang, Y. He, Y. Jiang, Y. Bian, Research on an Mg–Zn alloy as a degradable biomaterial, *Acta Biomater.* 6 (2010) 626–640. doi:10.1016/J.ACTBIO.2009.06.028.
- [104] R.-C. Zeng, X.-T. Li, S.-Q. Li, F. Zhang, E.-H. Han, In vitro degradation of pure Mg in response to glucose, *Sci. Rep.* 5 (2015) 13026. doi:10.1038/srep13026.
- [105] Chemical Equilibrium Diagrams | KTH. <https://www.kth.se/che/medusa/>.

Figure captions

Fig. 1. – PDP curves for the MA8 Mg alloy in MEM and 0.83 % NaCl solutions recorded after 60 min of immersion.

Fig. 2. – The evolution of the open circuit potential (60 min) for the MA8 samples in MEM and in NaCl solution.

Fig. 3. – The evolution of the EIS spectra (Nyquist plot (a), Bode plot (b)) with time of the MA8 magnesium alloy sample exposure to the NaCl solution. The spectra include experimental data marked by symbols (scatter plot) and theoretical fitting curves (solid line), which simulate the experimental data using equivalent electrical circuit (c). The arrows in (a) show the next spectrum (in time).

Fig. 4. – The evolution of the EIS spectra (Nyquist plot (a), Bode plot (b)) with time of the MA8 magnesium alloy sample exposure to the MEM. The spectra include experimental data marked by symbols (scatter plot) and theoretical fitting curves (solid line), which simulate the experimental data using equivalent electrical circuit (c). The arrows in (a) show the next spectrum (in time).

Fig. 5. – Impedance modulus (measured at the lowest frequency $|Z|_{f=0.1\text{Hz}}$) evolution during sample immersion in NaCl solution and in MEM.

Fig. 6. – The plot of the calculated parameters of the EEC element (C_1 and R_1) (Tables 2) for the sample during 74 h immersion in NaCl solution.

Fig. 7. – The plot of the calculated parameters of the EEC element (C_1 , C_2 , R_1 and R_2) (Tables 3) for the sample during 74 h immersion in MEM.

Fig. 8. – Optical images of the sample surface after 40 (a) and 64 (b) h of specimen exposure to MEM, which confirm the degradation of the surface film between two time-points.

Fig. 9. – The evolution of the open circuit potential with time (110 h) for the MA8 samples immersed in MEM or 0.83 % NaCl solution.

Fig. 10. – The investigated area (a) and acquired average Raman spectrum (b) of the MA8 Mg alloy sample after 30 days of immersion in MEM.

Fig. 11. – SEM-EDX maps of the cross-section of the MA8 Mg alloy sample after 30 days of immersion in MEM: SEM (a) and SEM-EDX (b) images of the corrosion film as well as corresponding EDX maps of the element distribution Mg (c), O (d), C (e), Ca (f), P (g).

Fig. 12. – SEM images of the sample cross-sections after 8 (a), 24 (b), 40 (c) and 64 (d) hours of the exposure to MEM. EDX maps of the element distribution O (c1), Ca (c2), P (c3) and Mg (d1), O (d2), Ca (d3), P (d4) in the corrosion film after 40 and 64 h of specimen exposure to MEM, respectively.

Fig. 13. – The schematic illustrations of the possible corrosion mechanism for MA8 Mg alloy in the MEM. Three stages (a, b, c) of the corrosion film evolution were revealed.

Fig. 14. – Inorganic species of MEM as a function of pH. Ions and concentrations correspond to their content in MEM. The diagram was made using Hydra/Medusa[®] software.